Intensity dependences of the nonlinear optical excitation of plasmons in graphene

T. J. Constant[1], S. M. Hornett[1], D. E. Chang[2], and E. Hendry[1]

[1]Electromagnetic Materials Group, Department of Physics, College of Engineering, Mathematics and Physical Sciences, University of Exeter, Exeter, Devon, UK. EX4 4QL.
[2]ICFO - Institut de Ciències Fotòniques, Mediterranean Technology Park, 08860 Castelldefels (Barcelona), Spain.

Recently, we demonstrated an all-optical coupling scheme for plasmons, which takes advantage of the intrinsic nonlinear optical response of graphene. Difference frequency mixing using free-space, visible light pulses generates surface plasmons in a planar graphene sample, where the phase matching condition can define both the wavevector and energy of surface waves and intraband transitions. Here, we also show that the plasmon generation process is strongly intensity dependent, with resonance features washed out for absorbed pulse fluences >0.1 J/m^2. This implies a subtle interplay between the nonlinear generation process and sample heating. We discuss these effects in terms of a nonequilibrium charge distribution using a two-temperature model.

Key index words: nonlinear optics, graphene, plasmonics

Graphene offers several beneficial properties as a plasmonics material, with excellent electro-optic tuneability[1], crystalline stability, large optical nonlinearities[2] and extremely high electromagnetic field concentration[3]. Yet, the extreme field confinement comes at a cost: wavevectors around two orders larger than free space radiation make surface plasmons very difficult to excite. This has led to the development of specialised measurement techniques, most of which rely on scattering resonances[4–6] or near-field sources[7,8]. However, the far-infrared region, the resonance region for graphene plasmons, lacks developed sources and detectors compared to the visible spectral domain. Moreover, for many future applications, including plasmonic circuits, it is particularity crucial to excite plasmon eigenstates with a singular energy, momentum and direction. It has recently been demonstrated[9] that one can employ an approach that can access a distinctly broad frequency range for surface plasmons in graphene, even down to the far infrared. This all-optical approach, involving the coherent excitation of surface plasmons using two visible frequency, free-space beams (referred to here as the "pump" and the "probe") via difference frequency generation (DFG), embodies many desirable aspects of directivity without requiring careful nanofabrication of antennas, with an estimated photon efficiency approaching 10^{-5}.

Here, we present intensity dependences of difference frequency coupling to surface plasmons in graphene. We show that the generation process is also strongly intensity dependent, with surface plasmon resonance features washed out for pulse fluences approaching 0.1 J/m^2, suggesting a subtle relationship between the plasmon generation process and sample heating. We also see a strong enhancement of the coherent signal when pump and probe beams are similar in energy. We discuss these intensity dependent effects in terms of a two-temperature model.

We begin by giving a brief overview of the experimental approach. Figure 1(a) shows our nonlinear coupling scheme illustrated on a dispersion diagram. By illuminating the graphene with two intense laser pulses with well-defined angles of incidence but different frequency, labeled f_{pump} and f_{probe}, one can phase match both the frequency and wavevector, k, of the surface plasmon. Similar approaches have been demonstrated experimentally for thin metallic films[10,11] and shown to be theoretically possible in a graphene film[12]. Such a second order wave mixing process is normally forbidden in centro-symmetric crystals[13], but possible in graphene because of the distinctively non-local, spatial character of the interaction[12, 14]. In the experiment, an identical pair of optical parametric amplifiers (OPAs), pumped by an amplified femtosecond laser system, generate 100 fs-pulses at a repetition rate of 1 kHz. The wavelengths of the two OPAs are selected independently, and the incident beams are weakly focused on the sample using 30 cm focal length lenses, giving rise to a very small uncertainty in angle ~ 0.017 rad, and a similarly negligible uncertainty for the in-plane wavevectors. Sets of half-waveplates and polarisers determine both the average power and polarisation. The incident pump pulse fluence used nominally set to ~1 J/m^2, and varied up to ~20 J/m^2, with a pump spot size on the sample of ~300 μm radius. Our pump fluence is more than an order of magnitude less than the photo-modification threshold for graphene[15, 16], while the probe fluence is typically up to two orders of magnitude smaller still. Absorbed fluences for the pump and probe beams, Φ_{pump} and Φ_{probe}, can be calculated from the incident angles and illumination area using Fresnel reflection and transmission functions, and is typically ~ 1% of the incident fluence.

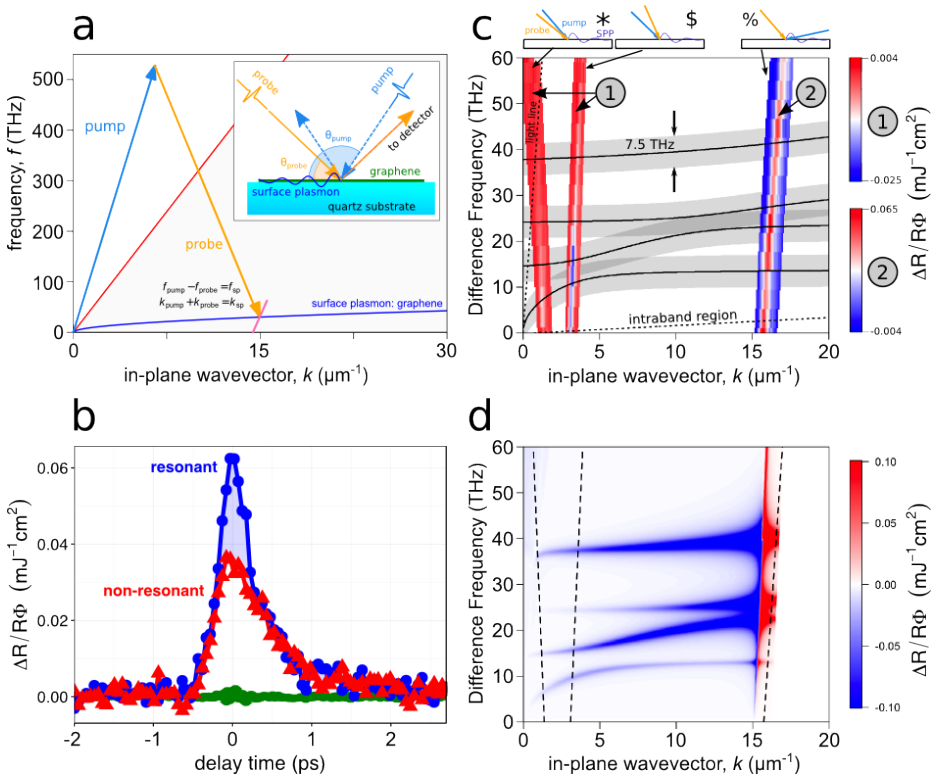

Figure 1 (Colour online). (a) The nonlinear coupling scheme illustrated on a dispersion diagram. The DFG of the pump and probe allows access to wavevectors outside of the light line. This permits phase-matching to the surface plasmon modes in graphene. The short (pink) line illustrates a region that can be interrogated by altering the pump wavelength from 615 nm to 545 nm with the probe wavelength fixed at 615 nm. (inset) The experimental arrangement used to excite surface plasmons on graphene. (b) Normalised differential reflection as a function of temporal overlap for the geometry θ_{pump} = 15°, θ_{probe} = 125°. At zero delay time, both the pump and probe pulses arrive simultaneously, leading to a nonlinear change in the probe reflection. Three curves are shown: The curve labeled "non-resonant" shows a typical time asymmetric measurement when the difference frequency produced by the pump and probe (56.3 THz) does not coincide with a surface plasmon energy state. The resonant curve shows an additional fast symmetric contribution to the recorded reflection signal when the difference frequency matches the energy of a graphene surface plasmon (23.8 THz). Note that there is no appreciable signal from the quartz substrate by itself: lower (green) line. (c) Plots of normalised differential reflection for three different experimental geometries, superimposed on the graphene surface plasmon-phonon dispersion (black lines). Incident angles (with respect to the substrate) are: [θ_{pump} = 55°,θ_{probe} = 45°], [$\$\theta_{pump}$ = 50°,θ_{probe} = 70°] and [$\%\theta_{pump}$ = 15°, θ_{probe} = 125°]. The intraband transition threshold and light line (dotted lines) are labeled on the diagram. The grey shading around the plasmon dispersion curve indicates the expected spectral broadening of the signals (~7.5 THz) due to the finite bandwidth of ~100 fs pulses. (d) The numerical solution for the normalised differential probe reflectance, calculated using the model outlined in text. The black dotted lines indicate the region of the dispersion relation probed by the experimental geometries shown in fig. 1(c).*

To obtain difference frequencies from from 0 to 60 THz, the pump wavelength is varied from 615 nm to 545 nm, with the probe wavelength set at 615 nm. We record the differential reflection of the probe beam defined as $\Delta R/R = (R - R_0)/R_0$, where R and R_0 are the reflections with and without the presence of the pump pulse, respectively, and recorded using a set of photo-balance diodes. In order to isolate the nonlinear reflection signal, we vary the temporal overlap of the two pulses using a motorised delay stage. Note that we normalise the signal by pump fluence in order to remove artifacts due to

power variation. Samples for our experiments are fabricated from commercially grown CVD graphene on copper foil (graphene supermarket). Transfer to quartz substrates was performed in house via a standard metal etching and float technique using Ammonium persulfate to etch the copper and PMMA as a support structure. Combined resistance and Raman spectroscopy[16, 17] give an estimated mobility of the samples of around 2000 cm^2/Vs and a natural Fermi energy of ~300 meV. Raman imaging indicates that the graphene is nominally single layer, with > 80% coverage of the substrate.

Results from the measurement of differential reflection are plotted in figures 1(b) and 1(c). For non-degenerate pump and probe beams, in addition to incoherent pump-induced changes in reflection, we observe wave mixing signals as a fast additional contribution to the signal, with a more symmetric lineshape, as seen in fig 1(b), where an absolute contribution to this signal is observed. Under "resonant" conditions (i.e. when phase matching conditions are satisfied), these coherent contributions can be up to four times the size of the incoherent contribution. Note that the temporal width of these symmetric contributions are broader than the incident femtosecond pulses due to temporal smearing caused by the finite spot size and non-normal incidence of the experimental geometry. When we vary the difference frequency, as in figure 1(c), we isolate resonant, coherent conditions. For the three different experimental geometries, we compare the measurement to the expected plasmon dispersion (black lines), calculated according to the model outlined in ref.[18], assuming a Fermi energy of 0.5 eV. This Fermi energy is larger than the expected intrinsic doping of our graphene samples, which we attribute to a significantly raised electron temperature expected under illumination by intense femtosecond pulses[19-23] (see later). Hybridisation with the substrate phonons leads to four branches, where we observe the maximum differential reflection. For larger difference frequencies, up to 150 THz, we do not observe any further resonance features in the spectra[9].

To understand the origin the couplings to different branches, we have developed a simple, quasi CW theoretical model that captures some of the features in figure 1(c), as described in ref.[9]. This simple model reproduces some of the salient features arising from different coupling efficiencies to different bands, with the highest coupling efficiency generally for the dispersion regions that are most 'plasmon-like' in origin. In addition to the surface plasmon resonance conditions, for the highest wavevector region in fig. 1(c) there is an additional resonant enhancement found in experiment at low frequencies < 5 THz. This signal lies within the expected region of intraband transitions in graphene, indicated by the dotted line in fig. 1(c). These intraband resonances are not included in our model. The assignment of most of the spectral features to surface plasmon excitation is further corroborated by the polarisation dependences presented in the supplementary material of ref. [9].

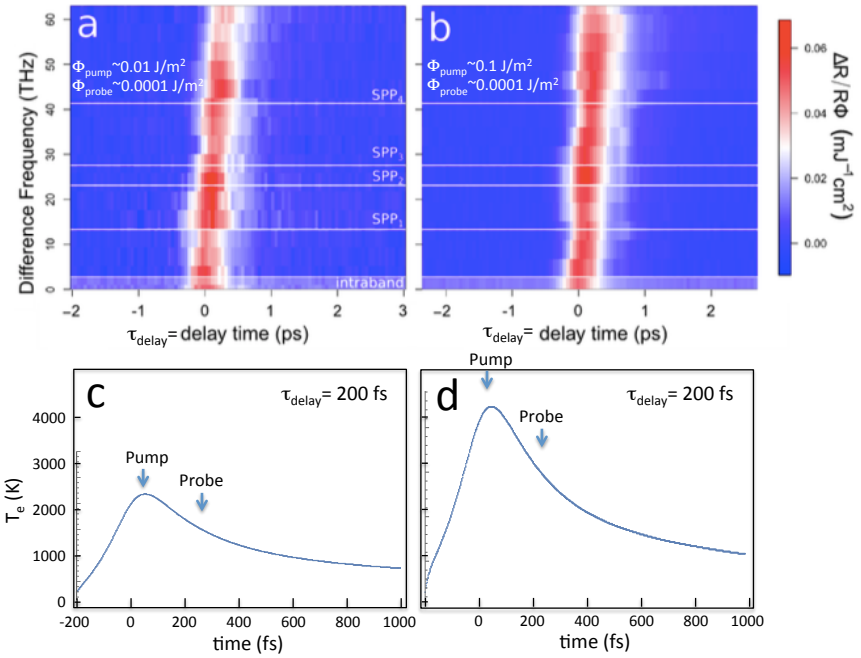

Figure 2 (Colour online). Upper panels: Differential reflection normalised to fluence as a function of temporal overlap for low (a) and high (b) pump fluences measured in geometry (%) from figure 1(c). Lower panels: electron temperature as a function of time, calculated according to the two-temperature model described in text, assuming the experimental absorbed fluences stated in the upper panels. The temperature is shown for a particular combination of pump and probe pulses separated in time by 200 fs (arrows). Note that, for this low probe fluence, the probe pulse has a negligible effect on the overall temperature.

Since the generation process is nonlinear by its very nature, one might expect a dependence on light intensity. While a complete investigation of the intensity dependences would be a laborious process requiring multiple parameter variation of both pulse intensities and wavelengths, which lies beyond the scope of this paper, we have carried out a limited investigation in this parameter space. Firstly, in order to investigate effects of electron heating, we first increase the absorbed pump fluence used in the experiment to ~0.1 J/m^2. The result of this intense excitation is compared to our earlier result in figure 2(a) and 2(b). Somewhat unexpectedly, we find that a higher fluence significantly suppresses the surface plasmon resonance features with respect to the background "non resonant" signal. It is the primary aim of this paper to understand the underlying physics behind this rather unexpected intensity effect. We begin by introducing model behavior for graphene under intense illumination. While we believe that our simple, continuous wave model for the coherent nonlinearity mentioned above captures some of the features of the effect in question, it is important to note that it completely ignores the non-equilibrium nature of excitation by intense femtosecond pulses. Heating effects from such intense illumination will affect both the coherent and incoherent contributions to our signal. Below, we first concentrate on the incoherent contribution to the signal, the intensity dependence of which can be elucidated using a relatively simple heating model. We then end with a brief discussion of the intensity dependence of the coherent contribution, which is much more problematic to describe.

We interpret the effects of pulse intensity on the incoherent contribution to our signals through effects of ultrafast heating, by introducing a simple two-temperature heating model that estimates the electron and optical phonon temperatures after

photoexcitation from ultrafast optical pulses. While such a simple model does ignore the truly dynamical and non-equilibrium nature of the electron distribution immediately after photoexcitation (see later), due to the very fast electron-electron scattering, it does give a reasonable description of a quasi-thermalized distribution of energy on the femtosecond timescale[19-22] and allows us to approximate the temperatures of the phonon and electron baths as a function of time after excitation. Briefly, this model, based on refs. [21,22] calculates the emission and absorption rates for phonons using the relation

$$\Gamma_{ph} = \alpha \int_{-\infty}^{+\infty} E(E - \hbar\omega_{ph}) \times [\rho_e - \rho_a] dE \,, \qquad [1]$$

where ω_{ph} is the optical phonon frequency (~180 meV), $\rho_e = f(E)[1 - f(E - \hbar\omega_{ph})](n_{ph} + 1)$ is the probability of emitting a phonon, $\rho_a = f(E - \hbar\omega_{ph})[1 - f(E)]n_{ph}$ is the probability of absorbing a phonon, n_{ph} is the phonon occupation number, and $f(E)$ is the Fermi- Dirac distribution of electrons for a given electron temperature, T_{el}. Here $\alpha = 9/2 \times \beta^2[\pi\rho\omega_{ph}\hbar^4 v_F^4]^{-1}$, is the electron-phonon coupling strength, where ρ is the density of graphene (~7.6 × 10−7 kg/m^2), v_F is the Fermi velocity, and β = 45 eV/nm [22]. The rates of phonon emission and absorption are, in turn, related to the electron and optical phonon temperatures, $T_{el}(t)$ and $T_{op}(t)$ through the coupled rate equations:

$$\frac{dT_{el}(t)}{dt} = \frac{I(t) - \Gamma_{ph}(T_{el}, T_{op})}{c_e(T_{el})},$$

$$\frac{dT_{op}(t)}{dt} = \frac{\Gamma_{ph}(T_{el}, T_{op})}{c_{op}(T_{op})} - \frac{T_{op}(t) - T_0}{\tau_{op}}, \qquad [2]$$

where τ_{op}~2 ps describes the anharmonic decay of optical phonons[21] and T_0 =300 K. We take the values for electron and electron and optical phonon specific heats, C_e and C_{op}, from ref. [22]. The function $I(t)$ describes the time dependence source of energy due to absorption of pump and probe pulses, and is given by [22]

$$I(t) = \frac{\Phi_{pump}}{2\tau_{exc}} \cosh^{-2}\left(\frac{t}{\tau_{exc}}\right) + \frac{\Phi_{probe}}{2\tau_{exc}} \cosh^{-2}\left(\frac{t - \tau_{delay}}{\tau_{exc}}\right), \qquad [3]$$

where τ_{exc} ~ 100 fs is the temporal width of the pulses, and τ_{delay} is the delay time between pump and probe pulses.

In figures 2(c) and 2(d) we plot the results of our two-temperature model for the absorbed fluences shown in the upper panels. For simplicity, we only show the time dependant electron temperature for a pump-probe time delay of 200 fs. We observe a rapid rise in the electron temperature to several thousand degrees K immediately following photoexcitation, followed by a fast decay due to coupling to optical phonons, similar to the behaviour observed previously with such models[21, 22], and similar also to the temporal dynamics of the incoherent contribution to this signal (see Fig. 1(b)). Note that, for this low probe fluence, the probe pulse has a negligible effect on the overall temperature. However, the pump fluence makes a significant difference, with a maximal electron temperature in 2(d) around a factor of two higher than for 2(c). As we discuss below, an increased electron temperature will alter the photoconductivity of the graphene, giving rise to the "incoherent" changes to the sample reflection.

Since we measure with two pulses, it is clear that the *relative* values for pump and probe intensities will also significantly affect the signal. In figures 3(a) and 3(b) we show differential reflection normalised to pump fluence for two difference frequencies, 0 THz

(λ_{pump} = 615 nm) and 12 THz (λ_{pump} = 600 nm), measured for geometry $, as defined in figure 1(c). In this geometry we expect a resonant enhancement for a difference frequency ~12 THz due to plasmon excitation. We compare the case for a high-power pump beam (absorbed fluence ~0.03 J/m^2) and a low power-probe beam (~0.003 J/m^2) to that when pump and probe fluences are approximately equal (~0.01 J/m^2). For approximately equal pump and probe fluences, as shown in figure 3 (b), we observe a significant suppression of the background, non-resonant signal. In this case, the coherent resonant signal more than three times the non-resonant, incoherent background signal. In figures 3(c) and 3(d) we again plot the electron temperature for the absorbed fluences shown in the upper panels, and for a pump-probe time delay of 200 fs. One sees, unsurprisingly, a larger probe fluence has a larger effect on the electron temperature. However, the change in temperature due to pulse absorption is clearly a saturable effect, since the change in temperature on absorption of the probe in 3(d) is smaller than that for absorption of the pump.

It is important how such elevated electron temperatures are expected to affect our experimental signals. In ref.[23] Dani et al demonstrated that for absorbed optical fluences < 3x10^{13} photons/cm^{-2} (corresponding to ~ 0.1 J/m^2), changes to the intraband conductivity determine the change in reflectance. Under such conditions, the change to the optical conductivity, and therefore δR, is expected to be approximately proportional to the change in electron temperature [23]. Since we record the change in reflectance of the probe pulse due to the presence of the pump pulse, the incoherent contribution to the signal is expected to be proportional to $\Delta T = T_{pump+probe} - T_{probe}$. In figure 3(e) we plot the maximum ΔT, calculated when pump and probe pulses are overlapped in time, as a function of absorbed pump and probe fluences. From this, it is clear that the pump-induced change in reflection coefficient of the probe due to heating *decreases* with increasing probe fluence. This observation explains why the incoherent background in figure 3(b) is considerably smaller than in 3(a). While the general trend (of a reduction in δR for a larger probe fluence) is reproduced in both the modelling and experiment, we note that this effect is stronger in experiment than in modelling: δR is predicted to decrease by factor of four in the model for the experimental fluences marked by (a) and (b), while in experiment it decreases by around a factor of seven (using the peak magnitudes of the blue curves in the upper panels). This discrepancy most likely arises due to inaccuracies in the electron and phonon heat capacities used in the calculation, which strictly apply only for zero Fermi level [22].

Finally, we consider the expected dependence of the coherent signal contribution. While our model suggests that the incoherent contribution to the signal is expected to diminish for increasing probe fluence, the coherent contribution is more problematic to describe, since we do not know the temperature dependence a priori. If we assume temperature independence of the mixing process, the intensity of the DFG frequency will be proportional to the product of pump and probe fluences. However, since we record the change in *reflectivity* of the probe, the experimental signal is expected to be proportional only to the pump fluence. Thus, for a factor of three reduction in the pump fluence, as recorded for figures 3(a) and (b), we also expect the reflectivity to decrease by a factor of three. However, we can see from the red lines in figures (a) and (b) that the reduction is less than expected. This indicates that heating effects are also important for this coherent signal. It is clear that, due to the negative photoconductivity usually exhibited by graphene for pulsed femtosecond excitation[20], one can expect increased losses and

quenching of the surface plasmon, leading to broadening of the spectral features associated with their excitation. We believe that this explains the "washing out" of the plasmon-associated features for high intensity photoexcitation in figure 2(b). This result points towards an optimal intensity regime for operation when excitation intensity is distributed evenly between pump and probe beams, as this leads to a lower temperature overall (see figure 3(d)).

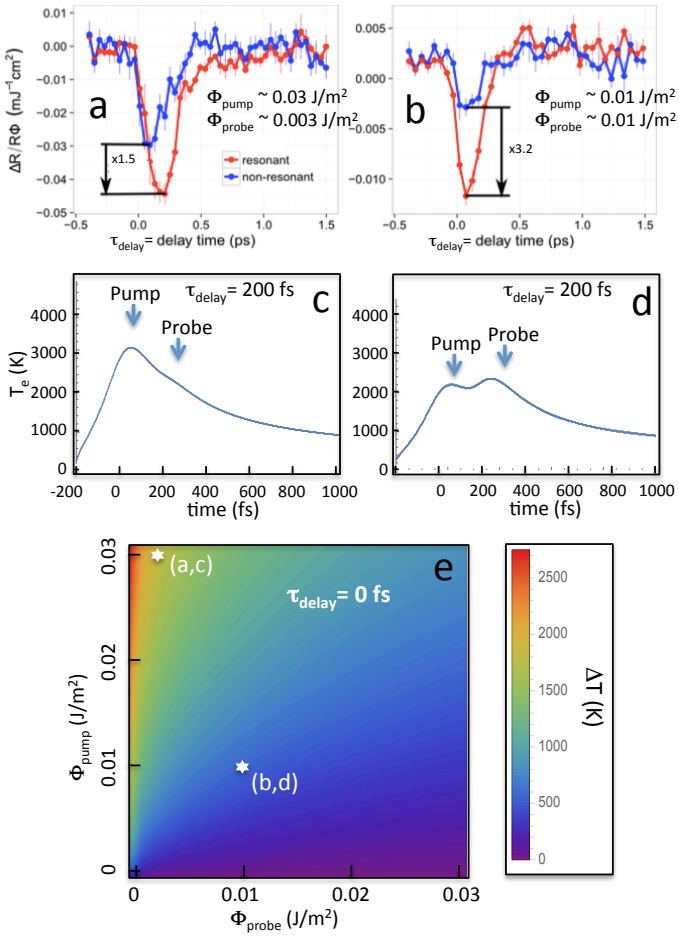

Figure 3 (Colour online). Upper panels: Differential reflection normalised to pump fluence as a function of temporal overlap of the pulses for: (a) high-fluence pump and low-fluence probe, and (b) comparable fluence in both pump and probe. The "non-resonant" lines indicate the case for the difference frequency of 0 THz (no resonant plasmon coupling) while the "resonant" lines are for a difference frequency of 12 THz (resonant plasmon coupling). Middle panels: electron temperature as a function of time, calculated according to the two-temperature model described in text, assuming the experimental absorbed fluences for the upper panels. Temperature is shown for a particular combination of pump and probe pulses separated in time by 200 fs, indicated with the arrows. Note that, for larger probe fluences, the probe pulse has a much greater effect on the overall temperature. Lower panel: (e) Maximum change in temperature ($\Delta T = T_{pump+probe} - T_{probe}$) calculated when pump and probe pulses are overlapped, as a function of absorbed pump and probe fluences, calculated according to the two-temperature model described in text. The white stars mark the combinations of pump and probe fluences measured and calculated in the upper panels.

In conclusion, we present intensity dependences of the nonlinear optical excitation of plasmons in graphene. We show that the plasmon generation process is strongly intensity dependent, with resonance features washed out for absorbed fluences of 0.1 J/m^2. We discuss the subtle interplay between the nonlinear generation process and

sample heating in terms of a simple two-temperature model, and suggest that optimal measurement conditions occur when intensity is distributed evenly between pump and probe beams. However, it is clear that to fully understand these subtly intertwined effects, modeling including the fully non-equilibrium electron distribution, which may lead to important effects such as plasmon stimulated emission and amplification[24], is required.

References

1. Craciun, M. F. F., Russo, S., Yamamoto, M. & Tarucha, S. Tuneable electronic properties in graphene. *Nano Today* **6,** 42–60 (2011).
2. Hendry, E., Hale, P. J., Moger, J., Savchenko, A. K. & Mikhailov, S. A. Coherent Nonlinear Optical Response of Graphene. *Phys. Rev. Lett.* **105,** 097401 (2010).
3. Brar, V. W., Jang, M. S., Sherrott, M., Lopez, J. J. & Atwater, H. A. Highly confined tunable mid-infrared plasmonics in graphene nanoresonators. *Nano Lett.* **13,** 2541–2547 (2013).
4. Gao, W. *et al.* Excitation and active control of propagating surface plasmon polaritons in graphene. *Nano Lett.* **13,** 3698–702 (2013).
5. Alonso-Gonzalez, P. *et al.* Controlling graphene plasmons with resonant metal antennas and spatial conductivity patterns. *Science (80-82).* **344,** 1369–1373 (2014).
6. Gao, W., Shu, J., Qiu, C. & Xu, Q. Excitation of plasmonic waves in graphene by guided-mode resonances. *ACS Nano* **6,** 7806–7813 (2012).
7. Fei, Z. *et al.* Gate-tuning of graphene plasmons revealed by infrared nano-imaging. *Nature* **487,** 82–85 (2012).
8. Chen, J. *et al.* Optical nano-imaging of gate-tunable graphene plasmons. *Nature* **487,** 77–81 (2012).
9. Constant, T. J., Hornett, S. M., Chang, D. E. & Hendry, E. All-optical generation of surface plasmons in graphene. *Nature Phys.* **12,** 124–127 (2016).
10. Renger, J., Quidant, R., van Hulst, N., Palomba, S. & Novotny, L. Free-Space Excitation of Propagating Surface Plasmon Polaritons by Nonlinear Four-Wave Mixing. *Phys. Rev. Lett.* **103,** 266802 (2009).
11. Palomba, S. *et al.* Nonlinear plasmonics at planar metal surfaces. (2011). doi:10.1098/rsta.2011.0100
12. Yao, X., Tokman, M. & Belyanin, A. Efficient nonlinear generation of THz plasmons in graphene and topological insulators . Supplemental material.
13. Boyd, R. W. *Nonlinear Optics*. (Elsevier, 2008).
14. Mikhailov, S. A. Theory of the giant plasmon-enhanced second-harmonic generation in graphene and semiconductor two-dimensional electron systems. *Phys. Rev. B - Condens. Matter Mater. Phys.* **84,** 1–6 (2011).
15. Brida, D. *et al.* Ultrafast collinear scattering and carrier multiplication in graphene. *Nat. Commun.* **4,** 1987 (2013).
16. E. Alexeev, J. Moger and E. Hendry, Photoinduced doping and strain in exfoliated graphene", Applied Physics Letters **103**, 151907 (2015).
17. Lee, J. E., Ahn, G., Shim, J., Lee, Y. S. & Ryu, S. Optical separation of mechanical strain from charge doping in graphene. *Nat. Commun.* **3,** 1024 (2012).
18. Luxmoore, I. J. *et al.* Strong Coupling in the Far-Infrared between Graphene Plasmons and the Surface Optical Phonons of Silicon Dioxide. *ACS Photonics* **1,**

1151–1155 (2014).
19. Jensen, S. A. *et al.* Competing Ultrafast Energy Relaxation Pathways in Photoexcited Graphene. *Nano Lett.* **14,** 5839–5845 (2014).
20. Tielrooij, K. J. *et al.* Photoexcitation cascade and multiple hot carrier generation in graphene. *Nat. Phys.* **9,** 248–252 (2013).
21. Hale P.J. *et al.* Hot phonon decay in supported and suspended exfoliated graphene. *Phys. Rev. B* **83**, 121404 (2011).
22. Lui C.H. *et al.* Ultrafast Photoluminescence from Graphene. *Phys. Rev. Lett.* **105**, 127404 (2010).
23. Dani K.M. *et al.* Intraband conductivity response in graphene observed using ultrafast infrared-pump visible-probe spectroscopy. *Phys. Rev. B* **86**, 125403 (2013).
24. Page, A. F. *et al.* Nonequilibrium plasmons with gain in graphene. *Phys Rev. B* **91**, 075404 (2015).

This research has been supported by the European Commission (FP7-ICT-2013-613024-GRASP) and EPSRC fellowship (EP/K041215/1).

Data this manuscript, and a Mathematica file to calculate the two-temperature model output, is available through https://ore.exeter.ac.uk/

Author contributions:
T.J.C. developed and carried out the experiments and data analysis, S.M.H. fabricated the samples and assisted with conceptual discussions, D.E.C. and E.H. developed the theoretical model and fitting of experimental data, and E.H. designed the experiment and assisted in data analysis and interpretation. All authors contributed to writing of the paper.